Spectrum-Efficient Coherent Optical OFDM for Transport Networks

Linglong Dai, Chao Zhang, Zhengyuan Xu, and Zhaocheng Wang

***Abstract*—Orthogonal frequency division multiplexing (OFDM) is a promising technology for the next-generation optical transmission systems beyond 100 Gb/s. To further improve the spectral efficiency and system reliability, we propose a flexible coherent zero padding OFDM (CO-ZP-OFDM) scheme with signaling-embedded preamble and polarization-time-frequency (PTF) coded pilots for high-speed optical transport networks. Our judicious design embeds signaling in the specially designed preamble whose Delta-like correlation function helps to simultaneously achieve very accurate timing and frequency synchronization. Unlike the periodically inserted training symbols, the PTF-coded pilots are properly distributed within the time-frequency grid of the ZP-OFDM payload symbols and used to realize low-complexity multiple-input multiple-output (MIMO) channel estimation at high accuracy. Compared with the conventional optical OFDM systems, CO-ZP-OFDM increases payload by about 6.68%, and the low-density parity-check (LDPC) coded bit error rate only suffers from no more than 0.3 dB compared with the back-to-back case even when the channel dispersion impairments are severe.**

***Index Terms*—Optical transport networks, coherent optical orthogonal frequency division multiplexing (CO-OFDM), polarization division multiplexing (PDM), multiple-input multiple-output (MIMO), zero padding OFDM (ZP-OFDM).**

I. Introduction

TRADITIONAL optical transport networks are often subject to the fixed ITU-T grid and frequency spacing, as well as spectrum over-provision for a low-rate optical channel [1], [2]. Enhancing the spectrum utilization is intensively demanded and becomes more challenging when next-generation optical transmission is evolving from 10 Gb/s to beyond 100 Gb/s [1]–[3]. The pioneering work by Shieh [4] has suggested coherent optical orthogonal frequency division multiplexing (CO-OFDM) to provide spectrum-efficient and elastic long-haul high-speed optical transmissions, whereas variable signal bandwidth and data rate could be easily and flexibly configured in a *gridless* fashion [4]–[8]. It is also demonstrated that CO-OFDM has superior tolerance to optical impairments including chromatic dispersion (CD) and polarization mode dispersion (PMD) [6], [7]. Moreover, high-order modulation and orthogonal-band-multiplexed (OBM) techniques can be easily supported by CO-OFDM to provide high-speed optical transmission even beyond Tb/s [3], [9], [10]. Furthermore, polarization division multiplexing (PDM) can be used jointly with CO-OFDM to double the throughput without increasing the signal bandwidth [6], [11], [12]. Therefore, PDM CO-OFDM is a promising candidate for next-generation high-speed optical transport networks.

One key feature of CO-OFDM is its superior tolerance to optical channel impairments including chromatic dispersion (CD) and polarization mode dispersion (PMD) [6], [7]. It has been proved that a PDM optical transmission link is essentially represented by a multiple-input multiple-output (MIMO) Jones matrix [6], [12]. Using periodically inserted training symbols, channel parameters are estimated and fed into a channel equalizer to compensate for the channel impairments. One effective design of training symbols is based on time-multiplexed single-polarization [12]–[14]. With multiple training symbols, time-domain averaging techniques can be applied to estimate the channel [3], [12]. A pair of correlated dual-polarization (CDP) training symbols are proposed to further improve the performance [15]. Without introducing extra overhead, the intra-symbol frequency-domain averaging (ISFA) method implements the neighboring subcarrier averaging in the same training symbol [16]. Moreover, the subcarrier/polarization interleaved symbols are proposed for frequency-domain channel estimation in [17]. However, those training based solutions did not fully utilize the specific properties of optical channels. First, the optical channel frequency response (CFR) is usually flat [12], [13], thus a small number of scattered subcarriers are sufficient for channel estimation, and there is no need for the training symbols to use all active subcarriers as pilots. Second, the interval between two adjacent training symbols is usually large, leading to the inaccurate channel tracking capability, especially when channel PMD may vary relatively fast [18]. Additionally, most CO-OFDM systems use cyclic prefix (CP) as the guard interval (we explicitly use the term "CO-CP-OFDM" in the rest part of the paper to stand for the conventional CO-OFDM scheme using CP as the guard interval), which does not carry data but consumes some transmit power.

To fully exploit the optical channel properties to achieve high spectral efficiency and reliable performance, we propose in the paper a flexible coherent optical zero-padding OFDM (CO-ZP-OFDM) transmission scheme based on signaling-embedded preamble and polarization-time-frequency (PTF) coded pilots. More specifically, we make the following contributions:

Manuscript received 25 December 2011; revised 30 August 2012. This work was supported by National Basic Research Program of China (973 Program) (No. 2013CB329203), National Natural Science Foundation of China (Grant Nos. 61132002, 61271266, 61201185), China Postdoctoral Science Special Foundation (Grant No. 2012T50093), Science and Technology Foundation for Beijing Outstanding Doctoral Dissertation Supervisor (Grant No. 20121000303), and Tsinghua University-KU Leuven Bilateral Scientific Cooperation Foundation (Grant No. BIL11/21T).

The authors are with Department of Electronic Engineering as well as Tsinghua National Laboratory for Information Science and Technology (TNList), Tsinghua University, Beijing 100084, P. R. China (e-mails: {daill, z-c, xuzy, zcwang}@tsinghua.edu.cn).

Digital Object Identifier 10.1109/JSAC.2013.130107.

0733-8716/13/$31.00 © 2013 IEEE

1) The flexible transmission frame structure to support variable system configurations. The CO-ZP-OFDM transmission frame is composed of one preamble and subsequent ZP-OFDM payload symbols, whereby ZP instead of CP is used as the guard interval to increase the power efficiency. Its parameters can be easily adjusted to meet various time-dependent traffic demands.

2) Signaling-embedded preamble for joint accurate timing/freqeuncy synchronization and signaling detection. To support CO-ZP-OFDM transmission, a special preamble is designed in both time and frequency domains to simultaneously achieve accurate timing synchronization based on the ideal Delta-like timing metric, accurate carrier frequency offset (CFO) estimation, as well as reliable signaling detection.

3) Spectrum-efficient PTF-coded pilots and the corresponding reliable PTF channel estimation. Unlike the periodically inserted training symbols used in most CO-CP-OFDM systems, our proposed PTF-coded pilots scattered within the time-frequency grid of the payload symbols help to significantly improve the spectral efficiency without sacrificing channel estimation accuracy. In addition, the pilot power boosting could further improve the channel estimation performance.

The remainder of this paper is organized as follows. The system model of the proposed CO-ZP-OFDM scheme is described in Section II. The corresponding CO-ZP-OFDM receiver design is presented in Section III. It illustrates in great detail preamble-based joint timing/frequency synchronization and signaling detection, pilot-based residual CFO and phase noise estimation, the PTF channel estimation using the PTF-coded pilots, channel equalization and LDPC decoding. Section IV studies the performance of the proposed scheme. Numerical results are shown in Section V. Finally, conclusions are drawn in Section VI.

Notation: We use the upper and lower boldface letters to denote matrices and column vectors, respectively; $\mathbf{0}_{M\times N}$ denotes the $M \times N$ zero matrix; $\mathbf{F}_N$ denotes the normalized $N \times N$ fast Fourier transform (FFT) matrix whose $(n+1, k+1)$th entry is $\exp(-j2\pi nk/N)/\sqrt{N}$; $(\cdot)^*$, $(\cdot)^T$, $(\cdot)^H$, $(\cdot)^{-1}$, and $|\cdot|$ denote the complex conjugate, transpose, Hermitian transpose, matrix inverse, and absolute operations, respectively; $\widehat{x}$ represents an estimate of x; $\text{angle}\{x\}$means the angle of the complex-valued x; Finally, $\widetilde{x}$ indicates that x is a frequency-domain signal.

II. CO-ZP-OFDM System Model

In this section, the system model of the proposed CO-ZP-OFDM scheme with low-density parity-check (LDPC) channel coding is first outlined. Then, three key components of the CO-ZP-OFDM transmitter, including the flexible transmission frame structure, the signaling-embedded preamble, as well as the PTF-coded pilots, are presented respectively in the following three subsections. Finally, the signal model of the CO-ZP-OFDM scheme over optical channels is presented.

A. CO-ZP-OFDM MIMO System Model

Figure 1 shows the overall system model of the proposed CO-ZP-OFDM MIMO scheme with LDPC channel coding.

At the transmitter side, two independent streams of input bits are encoded by different (n, k_i) LDPC encoders with the code rate $r_i = k_i/n$, wherein k_i is the number of useful information bits for the i-polarization (here $i = x, y$), and n denotes the output codeword length for both polarizations. The codeword is fed to the interleaver before serial-to-parallel (S/P) conversion, and then constellation mapping is applied symbol by symbol. The PTF-coded pilots (will be addressed in detail in Section II-D) are multiplexed with the useful data in the frequency domain, and inverse fast Fourier transform (IFFT) is used to generate the time-domain OFDM symbol. The preamble (will be addressed in detail in Section II-C) is inserted for timing/frequency synchronization and signaling detection. As the guard interval, ZP is added at the end of the preamble and all OFDM symbols to generate the CO-ZP-OFDM transmission frame. After parallel-to-serial (P/S) conversion, the baseband ZP-OFDM signals in the x-polarization (I_x, Q_x) and y-polarization (I_y, Q_y) are fed to the digital-to-analog converter (DAC). Its output signal is modulated onto an optical carrier in an optical IQ modulator composed of two Mach-Zehnder modulators (MZM) with 90^{o} phase shift [7]. Finally, a polarization-beam splitter (PBS) is used for polarization multiplexing. In the fiber transmission link, the erbium-doped fiber amplifier (EDFA) is used for signal amplification after each fiber span so that the fiber loss can be roughly compensated for.

At the receiver side, the received signal is split into two random polarizations and then detected by the polarization-diversity optical hybrid detector, whose outputs are fed to the analog-to-digital converter (ADC) to identify the digitalized baseband signals $I_x^{'}$, $Q_x^{'}$, $I_y^{'}$, and $Q_y^{'}$. The specially designed preamble is used for joint timing/frequency synchronization and signaling detection. Then the ZP-OFDM signals are converted back into the frequency domain to separate the PTF-coded pilots and useful data. The PTF channel estimation based on the PTF-coded pilots is performed so that channel equalization of the useful data could be realized. Subsequently, constellation demapping, P/S conversion, de-interleaving, and LDPC decoding are sequentially implemented to recover the transmitted bits.

Three key components of the proposed CO-ZP-OFDM transmitter, namely, the flexible transmission frame structure, signaling-embedded preamble, and the PTF-coded pilots, will be discussed in the following three subsections, respectively.

B. Flexible CO-ZP-OFDM Transmission Frame Structure

Figure 2 compares the frame structure of the conventional CO-CP-OFDM systems with that of the proposed CO-ZP-OFDM scheme for optical transport networks.

For most CO-CP-OFDM systems, as shown in Fig. 2 (a), the transmission frame is composed of CP-OFDM symbols, wherein each symbol uses CP as the guard interval. The preamble at the beginning of each transmission frame is used for timing/frequency synchronization, and the training symbols with all active subcarriers used as pilots are periodically inserted among CP-OFDM payload symbols to estimate the

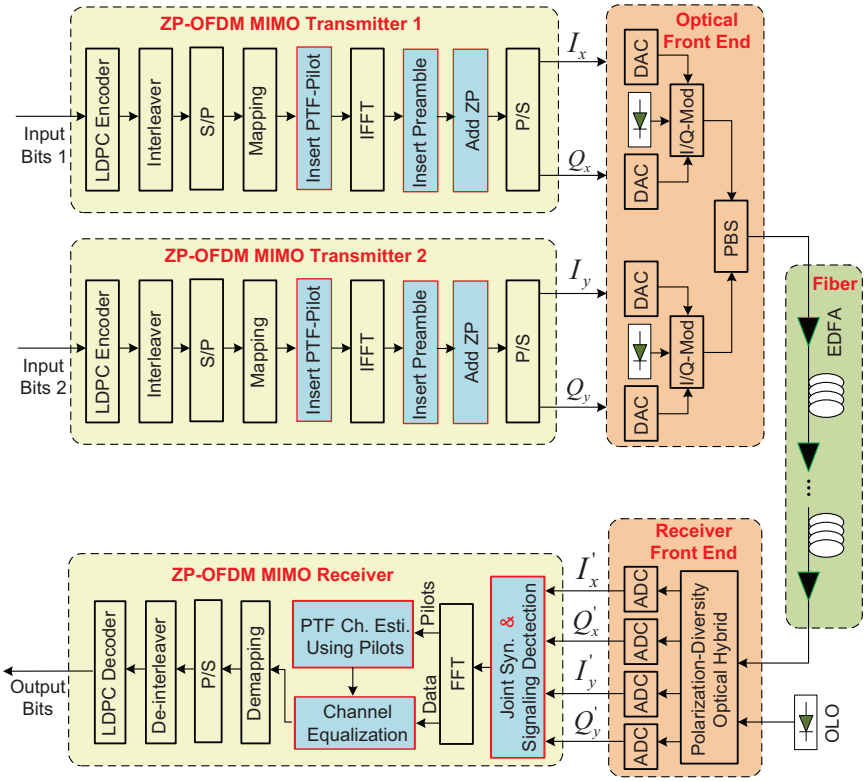

Fig. 1. System model of the proposed CO-ZP-OFDM scheme with PDM and LDPC channel coding.

channel between two adjacent training symbols.[1] In addition, some extra subcarriers in the payload symbols are used as pilots for residual CFO and phase noise estimation.

However, as shown in Fig. 2(b), the proposed CO-ZP-OFDM transmission frame is composed of one specially designed signaling-embedded preamble and the followed ZP-OFDM payload symbols containing the PTF-coded pilots. The ith ZP-OFDM symbol $\mathbf{z}_x^{(i)} = [z_{0,x}^{(i)}, z_{1,x}^{(i)}, \cdots, z_{N+M-1,x}^{(i)}]^T$ in the x-polarization consists of the IFFT data block $\mathbf{s}_x^{(i)} = [s_{0,x}^{(i)}, s_{1,x}^{(i)}, \cdots, s_{N-1,x}^{(i)}]^T$ of length N and the followed zero padding of length M, i.e.,

$$\mathbf{z}_x^{(i)} = \left[\left(\mathbf{s}_x^{(i)}\right)^T \mathbf{0}_{M\times 1}^T\right]^T, \tag{1}$$

where $\mathbf{s}_x^{(i)} = \mathbf{F}_N^H \widetilde{\mathbf{s}}_x^{(i)}$ is obtained by applying IFFT to the frequency-domain data $\widetilde{\mathbf{s}}_x^{(i)} = [\widetilde{s}_{0,x}^{(i)}, \widetilde{s}_{1,x}^{(i)}, \cdots, \widetilde{s}_{N-1,x}^{(i)}]^T$, which may contain some useful data and some pilots. Similarly, the IFFT data block of the ith ZP-OFDM symbol in the y-polarization can be denoted by $\mathbf{s}_y^{(i)} = \mathbf{F}_N^H \widetilde{\mathbf{s}}_y^{(i)}$. The proposed CO-ZP-OFDM differs from the conventional CO-CP-OFDM in three aspects. First, every symbol (including the preamble) within the transmission frame utilizes ZP instead of CP as the guard interval to improve the power efficiency. Second, a new signaling-embedded preamble is designed to achieve more accurate timing/frequency synchronization, and the system parameter signaling can be carried by the preamble as well. Third, without periodically inserted training symbols, the PTF-coded pilots scattered within the time-frequency grid are proposed to achieve reliable channel estimation as well as residual CFO and phase noise compensation.

Additionally, to further enhance the system flexibility and improve the spectrum efficiency for future optical transport

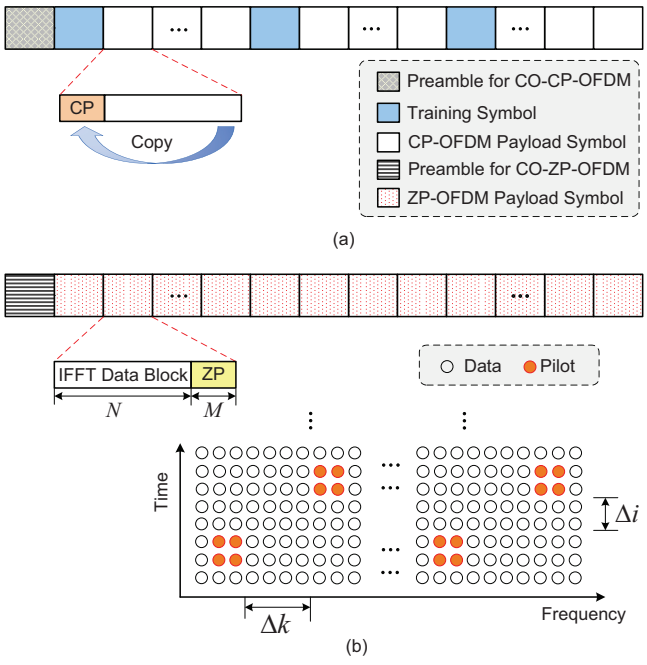

Fig. 2. Frame structure for optical OFDM block transmission: (a) Conventional CO-CP-OFDM; (b) Proposed CO-ZP-OFDM.

[1]Alternatively, unlike the periodical insertion scheme where a pair of training symbols are used after every 20 CP-OFDM symbols in [16], all the training symbols can also be put together directly after the preamble, e.g., 32 training symbols are located at the beginning of the transmission frame having 500 CP-OFDM symbols in [14].

networks, the flexible CO-ZP-OFDM frame structure could support a number of working modes with different payload symbol number K (e.g., K could be 300 [17] or 500 [14]), IFFT size N (e.g., N could be 512, 1024, 2048, etc.), guard interval length M (e.g., M could be $N/32$, $N/16$, $N/8$, etc.), constellation modulations (e.g., BPSK, QPSK, 16QAM, etc.), channel coding schemes (e.g., convolutional code, Turbo code, LDPC code, etc.), code rates (e.g., 0.6, 0.8, 0.9, etc.), and so on. Note that the 8-bit signaling could support 256 different working modes. Those system parameters can be flexibly configured so that spectrum-efficient and elastic optical transport networks can be realized according to the time-dependent traffic demand. They may vary frame by frame, or even within the same frame, e.g., different IFFT sizes can be supported in one transmission frame, and different constellation modulations can be used even in a certain ZP-OFDM payload symbol. Without loss of generality, this paper assumes that the system parameters are configured per frame basis. Usually some dedicated resources are required to reliably transmit those important system parameters, e.g., 36 subcarriers in every OFDM symbol are used in [19]. However, we design a signaling-embedded preamble to jointly realize timing/freqnecy synchronization and signaling detection in the next subsection.

C. Signaling-Embedded Preamble

In most CO-CP-OFDM systems, the preamble at the beginning of the transmission block is used for timing synchronization and CFO estimation [13], [14], [17]. The most widely used preamble is the one proposed by Schmidl [17], [20], but it suffers from performance degradation since the timing metric used for synchronization has a plateau even over single-path channels. This problem can be resolved by Minn's preamble [14], [21], wherein multiple repetitive parts with specifically designed signs yield a well-behaved timing metric, but the timing metric of the Minn's preamble is not sharp enough to acquire the exact timing of the transmission block, and the CFO estimation accuracy is reduced [21].

In this paper, we propose a novel signaling-embedded preamble design to simultaneously achieve the following three merits: 1) Ideal Delta-like timing metric for very accurate timing synchronization; 2) Accurate CFO estimation for a large range of parameters; 3) System parameter signaling transmission. The proposed preamble structures in the frequency and time domains are illustrated by the top and bottom parts of Fig. 3, respectively.

In the frequency domain, the preamble $\widetilde{\mathbf{p}} = [\widetilde{p}_0, \widetilde{p}_1, \cdots, \widetilde{p}_{N-1}]^T$ of length N is composed of three distinct parts: 1) Two guard bands filled with zero subcarriers are located at high frequency band and low frequency band (including the DC subcarrier), and each guard band has g_0 subcarriers; 2) Two identical Hadamard sequences occupy two separated regions with the distance of Δd, and each region has 2^{n+1} subcarriers; 3) In the middle, Δd zero subcarriers are used to separate the two Hadamard sequences.

The Hadamard sequence $\widetilde{\mathbf{u}}$ of length 2^n is extracted from any column of the n-order real-valued Hadamard matrix $\mathbf{H}_n$

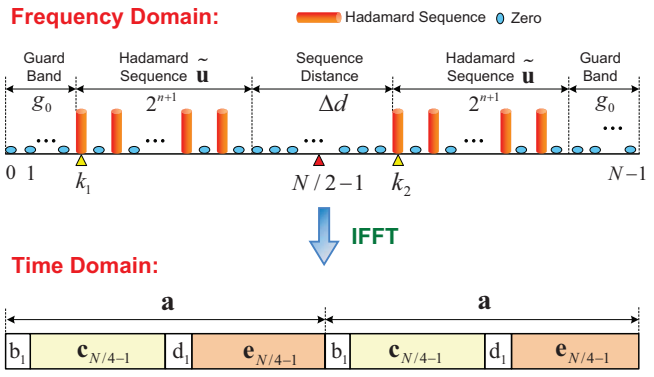

Fig. 3. Frequency-domain and time-domain structures of the signaling-embedded preamble.

recursively generated by

$$\mathbf{H}_1 = \begin{bmatrix} +1 & +1 \\ +1 & -1 \end{bmatrix}_{2\times 2}, \mathbf{H}_n = \begin{bmatrix} +\mathbf{H}_{n-1} & +\mathbf{H}_{n-1} \\ +\mathbf{H}_{n-1} & -\mathbf{H}_{n-1} \end{bmatrix}_{2^n \times 2^n}. \tag{2}$$

Then, the Hadamard sequence $\widetilde{\mathbf{u}} = \{\widetilde{u}_k\}_{k=0}^{2^n-1}$ is mapped on the even subcarriers of two regions with the frequency-domain distance Δd as below

$$\widetilde{p}_k = \begin{cases} \widetilde{u}_{(k-k_1)/2}, & \mathrm{mod}(k,2) = 0, k_1 \le k < k_1 + 2^{n+1}, \\ \widetilde{u}_{(k-k_2)/2}, & \mathrm{mod}(k,2) = 0, k_2 \le k < k_2 + 2^{n+1}, \\ 0, & \text{others}, \end{cases} \tag{3}$$

where $k_1 = g_0 + \Delta d/2$, and $k_2 = k_1 + 2^{n+1} + \Delta d$.

Unlike conventional preambles mainly used for time/frequency synchronization, we propose to embed the system signaling in the preamble so that no extra dedicated overhead will be required to carry the system parameters. This is achieved by the combination of selected Hadamard sequence and the specific sequence distance according to the configured signaling. More specifically, different signaling corresponds to distinct Hadamard sequences and/or sequence distances, both of which could be detected by the receiver to recover the transmitted signaling. First, when one specific Hadamard sequence $\widetilde{\mathbf{u}}$ has been selected, one specific sequence distance Δd could convey certain signaling. For example, in Fig. 3 we assume the following values $N = 2048, 2^{n+1} = 512, g_0 = 128$, so the value of Δd could be configured to vary within the range $(256, 768]$ (the minimum sequence distance $\Delta d_{\min}$ should be larger than zero, e.g., 256 mentioned here, so virtual subcarriers located in the middle of the signal bandwidth can be used to alleviate the carrier leakage effect [22]). Bear in mind that only the even subcarriers are used in the preamble, Δd should be an even number, so the distance range $(256, 768]$ could carry 8-bit signaling (notice that $(768 - 256)/2 = 2^8$). Second, since Δd can carry no more than 9-bit signaling even when $g_0 = 0$ and $\Delta d_{\min} = 0$, more signaling bits could be provided by selecting different Hadamard sequences. For example, the signaling bits could be increased from 8 to 10 if four possible Hadamard sequence candidates can be used. The receiver can easily identify which one is selected due to the orthogonality of different Hadamard sequences. Since sequence discrimination via correlation has higher complexity

than sequence distance detection, using sequence distance to carry signaling is preferred if the sequence distance could provide the required signalling bits. Note that if no signaling is embedded in the preamble, the fixed Hadamard sequence $\widetilde{\mathbf{u}}$ and sequence distance Δd will be assigned.

In the time domain, the preamble $\mathbf{p} = [p_0, p_1, \cdots, p_{N-1}]^T$ is obtained by applying IFFT to the frequency-domain preamble $\widetilde{\mathbf{p}}$, yielding

$$\mathbf{p} = \alpha \mathbf{F}_N^H \widetilde{\mathbf{p}}, \tag{4}$$

where α is a power scaling factor to make the preamble have the same average power as data symbol with N subcarriers, e.g., $\alpha = \sqrt{N/2^{n+1}}$. It takes the following form

$$\mathbf{p} = [\underbrace{\mathrm{b}_1 \ \mathbf{c}_{N/4-1} \ \mathrm{d}_1 \ \mathbf{e}_{N/4-1}}_{\mathbf{a}} \underbrace{\mathrm{b}_1 \ \mathbf{c}_{N/4-1} \ \mathrm{d}_1 \ \mathbf{e}_{N/4-1}}_{\mathbf{a}}]^T, \tag{5}$$

where $\mathbf{a} = [\mathrm{b}_1 \ \mathbf{c}_{N/4-1} \ \mathrm{d}_1 \ \mathbf{e}_{N/4-1}]$ of length $N/2$ is composed of four parts: both b_1 and d_1 have only one entry, while $\mathbf{c}_{N/4-1}$ and $\mathbf{e}_{N/4-1}$ have the length of $N/4-1$. Compared with Schmidl's and Minn's preambles [20], [21], the proposed preamble $\mathbf{p}$ simultaneously enjoys the following two time-domain features: 1) Similar to Schmidl's design, $\mathbf{p}$ is also composed of two identical time-domain parts, e.g., $\mathbf{p} = [\mathbf{a} \ \ \mathbf{a}]^T$, because only the even subcarriers are occupied by non-zero signals in the frequency domain; 2) Meanwhile, within part $\mathbf{a}$, $\mathbf{c}_{N/4-1}$ and $\mathbf{e}_{N/4-1}$ are conjugate symmetric, i.e.,

$$c_n^* = e_{N/4-1-n}, \quad 0 \le n \le N/4-1. \tag{6}$$

The first feature is useful for accurate CFO estimation, and the second one is essential for accurate timing synchronization, both of which will be addressed in detail in Section III-A.

D. Polarization-Time-Frequency Coded Pilots

For most CO-CP-OFDM systems, channel estimation is realized by the periodically inserted training symbols, whereby all active subcarriers are used as pilots, and the insertion period is relatively large to avoid too much overhead. However, this scheme does not fully utilize the optical channel properties, and sacrifices the spectral efficiency. We propose the PTF-coded pilots scattered within the time-frequency grid of the ZP-OFDM payload symbols to increase the spectral efficiency and improve the channel estimation performance as well.

As illustrated in Fig. 4 (here, only one time-frequency block is presented, since other blocks share the identical pilot pattern with the one shown in this figure), the PTF-coded pilots for the proposed CO-ZP-OFDM scheme can be explained from the following four aspects:

1) *Four-pilot cluster*. As illustrated in Fig. 4, the pilots appear in cluster, wherein each cluster is composed of four adjacent pilots in the time-frequency grid with the frequency-domain distance Δk and time-domain distance Δi. Since the optical channel usually has flat frequency response and slow time-variation [23], Δk and Δi could be large, e.g., $\Delta k = 8$ and $\Delta i = 8$ can be used when $N = 2048$. Note that different values of Δk and Δi could be configured to enhance the system flexibility (e.g., $\Delta k = 2$ and $\Delta i = 0$ are used in Fig. 4 for simplicity).

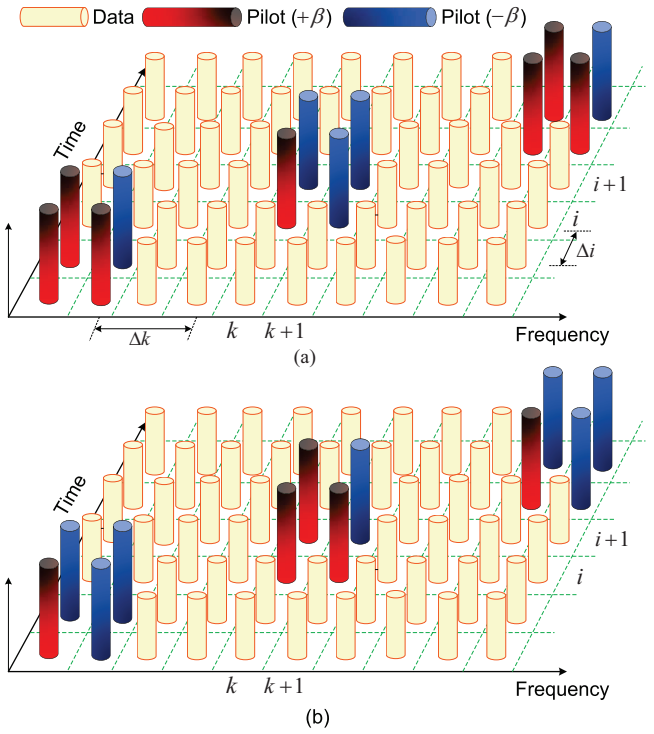

Fig. 4. Polarization-time-frequency (PTF) coded pilots scattered within the time-frequency grid of the ZP-OFDM payload symbols in the proposed CO-ZP-OFDM scheme with PDM: (a) Pilots in the x-polarization; (b) Pilots in the y-polarization.

2) *Polarization-time orthogonal pilots*. In the polarization-time domain, for the kth subcarriers in the ith and $(i+1)$th ZP-OFDM symbols in both x-polarization and y-polarization (the corresponding pilots extracted from Fig. 4 are then shown in Fig. 5), the pilots take the form

$$\begin{bmatrix} \widetilde{p}_{k,x}^{(i)} & \widetilde{p}_{k,x}^{(i+1)} \\ \widetilde{p}_{k,y}^{(i)} & \widetilde{p}_{k,y}^{(i+1)} \end{bmatrix} = \begin{bmatrix} a & c \\ b & d \end{bmatrix}, \tag{7}$$

where $\widetilde{p}_{k,x}^{(i)}$ denotes the pilot in the x-polarization on the subcarrier k in the ith ZP-OFDM symbol. The pilots in (7) can be selected from the standard constellations (e.g., BPSK, QPSK, 16QAM) and the pilots in each cluster should be orthogonal, i.e., $ac^* + bd^* = 0$. Figure 6 provides an example on the pilot cluster selection when BPSK, QPSK, and 16QAM constellations are used.[2] For the simplest form when BPSK constellation is used, $a = b = d = 1, c = -1$ can be used without loss of generality, even though other choices exist such as $a = b = c = 1, d = -1$.

3) *Polarization-frequency orthogonal pilots*. In the polarization-frequency domain, for the ith ZP-OFDM symbol, the pilots on the kth and $(k+1)$th subcarriers in the x-polarization and y-polarization follow the form of

$$\begin{bmatrix} \widetilde{p}_{k,x}^{(i)} & \widetilde{p}_{k+1,x}^{(i)} \\ \widetilde{p}_{k,y}^{(i)} & \widetilde{p}_{k+1,y}^{(i)} \end{bmatrix} = \begin{bmatrix} a & c \\ b & d \end{bmatrix}, \tag{8}$$

[2]Note that other choices to make the pilots within the cluster orthogonal also exist.

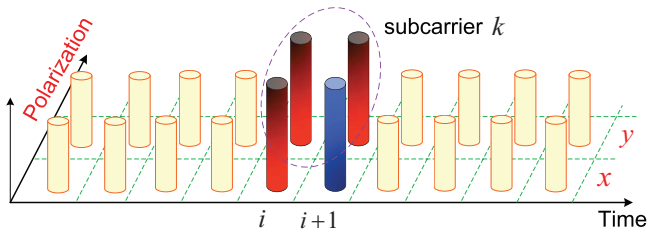

Fig. 5. Polarization-time orthogonal pilots. This figure is directly derived from Fig. 4 (a) and Fig. 4 (b) presenting the pilots in the x-polarization and y-polarization, respectively.

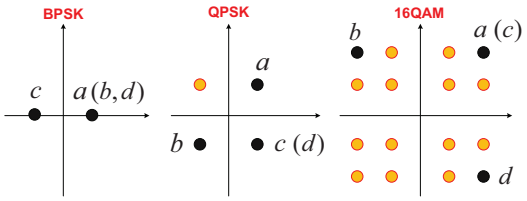

Fig. 6. Examples of the pilot pattern selection when BPSK, QPSK, and 16QAM constellations are used.

where the pilots in each cluster are also orthogonal (i.e., $ac^* + bd^* = 0$), which can be achieved similarly to that in (7).

Combining (7) and (8), we can find that the proposed pilot cluster has orthogonal pilots both in the polarization-time and polarization-frequency domains. For this reason, the term "PTF-coded pilots" is used throughout the paper.

4) *Pilot power boosting*. It is optional to make the average pilot power higher than the useful data power to enhance the channel estimation performance. More specifically, compared with the useful data, the amplitude of the pilots can be boosted by a factor of β, e.g., $\beta = \sqrt{2}$, $\beta = 2$, $\beta = 2\sqrt{2}$, etc. As mentioned above, only a small number of PTF-coded pilots suffices to track the optical channel, so insignificant optical signal-to-noise ratio (OSNR) penalty at the receiver will be caused by the boosted pilot power.

E. Signal Model over Optical Channels

After transmission through the optical link, the nth received time-domain sample $\mathbf{r}_n^{(i)} = [r_{n,x}^{(i)}\ r_{n,y}^{(i)}]^T$ corresponding to the transmitted signal $\mathbf{s}_n^{(i)} = [s_{n,x}^{(i)}\ s_{n,y}^{(i)}]^T$ in the ith ZP-OFDM symbol should be [23]

$$\mathbf{r}_n^{(i)} = e^{j\phi^{(i)}} \sum_{l=0}^{L-1} \mathbf{H}_l^{(i)} \mathbf{s}_{n-l}^{(i)} + \mathbf{w}_n^{(i)}, \tag{9}$$

where $\phi^{(i)}$ is the phase noise caused by the unmatched transmit and receive lasers, $\mathbf{H}_l^{(i)}$ denotes the 2×2 channel impulse response (CIR) matrix of the lth path including the optical impairment effects like CD, PMD, and polarization dependent loss (PDL) [23], L denotes the channel length, which should be smaller than the ZP length to combat the inter-symbol-interference (ISI) introduced by CD and PMD, and $\mathbf{w}_n^{(i)}$ denotes a vector with every element being the additive white Gussian noise (AWGN) dominated by the amplified spontaneous emission (ASE).[3]

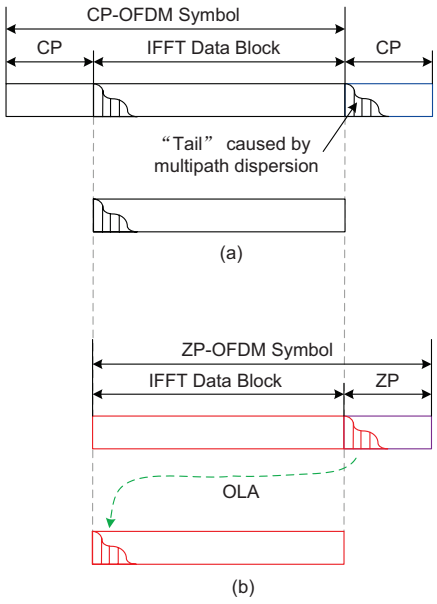

Fig. 7. Comparison of cyclicity reconstruction for CP-OFDM and ZP-OFDM symbols: (a) Cyclicity reconstruction is directly achieved by removing CP at the CP-OFDM receiver; (b) Cyclicity reconstruction is accomplished by OLA processing at the ZP-OFDM receiver.

As illustrated in Fig. 7, when the optical channel is time-invariant during one ZP-OFDM symbol,[4] the received IFFT data block in ZP-OFDM is essentially the same as that in CP-OFDM after overlap-and-add (OLA) processing used to reconstruct the cyclicity of the received IFFT data block [25], whereby the "tail" caused by the multipath effect is added to the front part of the received IFFT data block.

Based on the essentially equivalent nature between CP-OFDM and ZP-OFDM after OLA processing [25], the received frequency-domain signal $\widetilde{\mathbf{r}}_k^{(i)} = [\widetilde{r}_{k,x}^{(i)}\ \widetilde{r}_{k,y}^{(i)}]^T$ corresponding to the transmitted signal $\widetilde{\mathbf{s}}_k^{(i)} = [\widetilde{s}_{k,x}^{(i)}\ \widetilde{s}_{k,y}^{(i)}]^T$ on the kth subcarrier in the ith ZP-OFDM symbol can be presented by [6], [12]

$$\widetilde{\mathbf{r}}_k^{(i)} = e^{j\phi^{(i)}} \widetilde{\mathbf{H}}_k^{(i)} \widetilde{\mathbf{s}}_k^{(i)} + \widetilde{\mathbf{w}}_k^{(i)}, \tag{10}$$

where

$$\widetilde{\mathbf{H}}_k^{(i)} = \begin{bmatrix} h_{k,xx}^{(i)} & h_{k,xy}^{(i)} \\ h_{k,yx}^{(i)} & h_{k,yy}^{(i)} \end{bmatrix} \triangleq \sum_{l=0}^{L-1} \mathbf{H}_l^{(i)} e^{-j\frac{2\pi}{N}lk} \tag{11}$$

is the MIMO Jones channel matrix [6].

III. CO-ZP-OFDM Receiver Design

This section studies CO-ZP-OFDM receiver design including the preamble-based joint timing/frequency synchronization

[3]The instantaneous noise is subject to Poisson distribution but can be well approximated as Gaussian, and the overall noise has the statistics of Gaussian distribution [24].

[4]Rigorously speaking, the optical channel is not time-invariant since PMD is a time-varying effect. However, the slowly-varying nature of PMD leads to the coherent time usually in the order of magnitude larger than practical ZP-OFDM symbol duration [23], thus the optical channel can be considered constant at least during one ZP-OFDM symbol.

and signaling detection, the pilot-based residual CFO and phase noise estimation, the PTF channel estimation using the PTF-coded pilots, and finally, channel equalization and LDPC decoding.

A. Preamble-Based Joint Timing/Frequency Synchronization and Signaling Detection

The specially designed preamble facilitates accurate timing/frequency synchronization as well as physical layer signaling transmission. Using the conjugate symmetric property of the preamble, the exact starting point d_0 of the ZP-OFDM frame is acquired by maximizing the timing metric $M(d)$ as below

$$d_0 = \arg\left\{\max_d\{M(d)\}\right\} = \arg\left\{\max_d\{\frac{|P(d)|^2}{R^2(d)}\}\right\}, \quad (12)$$

where

$$P(d) = \sum_{n=1}^{N/2-1} q_{d+n}^* q_{N+d+n}, \quad (13)$$

denotes the correlation function of the received preamble $\{q_n\}_{n=0}^{N-1}$, and

$$R(d) = \sum_{n=1}^{N/2-1} |q_{d+n}|^2 \quad (14)$$

represents the average power of the received preamble used to normalize the correlation function $P(d)$ in (13).

After timing synchronization, CFO estimation (or frequency synchronization) should be performed before further processing. In CO-ZP-OFDM systems with intradyne receiver front end, the CFO Δf between the local optical laser oscillator (OLO) and the incoming signal is at most equal to the OFDM symbol rate $1/T$ (or one subcarrier spacing) [24], i.e., the normalized CFO denoted by $\Omega = \Delta f T$ satisfies $|\Omega| \leq 1$ (CFO in optical OFDM systems is most likely to be about 10%-20% of one subcarrier spacing [24], so $|\Omega| \leq 0.2$ is usually valid). Thus, the receiver only needs to perform the fine (fractional) CFO estimation. Similar to Schmidl's method [20], the CFO estimate $\widehat{\Omega}$ can be obtained by exploiting the time-domain structure of the proposed preamble with two identical halves as below

$$\widehat{\Omega} = \frac{1}{\pi}\text{angle}\left\{P'(d_0)\right\}, \quad (15)$$

where

$$P'(d_0) = \sum_{n=0}^{N/2-1} q_{d_0+n}^* q_{N/2+d_0+n}. \quad (16)$$

Due to the phase ambiguity issue, the estimation range of (15) is $(-1, +1]$, which is sufficient for CO-ZP-OFDM systems since only the fine CFO estimation is required as mentioned above. On the other hand, the proposed preamble can also deal with CFO much larger than one subcarrier spacing, e.g., by exploiting the property that the integral CFO results in the frequency-domain shifting of the active subcarriers but can be easily determined by comparing the received preamble with the local known preamble in the frequency domain.

Notice that, the correlation function $P'(d_0)$ in (16) is used for both timing and frequency synchronization in Schmidl's method [20], while $P'(d_0)$ is only used for CFO estimation but $P(d_0)$ in (12) is used for timing synchronization in our proposed scheme.

After timing synchronization and CFO compensation, the OLA method [25] is applied to reconstruct the cyclicity of the received time-domain preamble $\{q_n\}_{n=0}^{N-1}$, which is then converted to the frequency-domain preamble $\{\widetilde{q}_k\}_{k=0}^{N-1}$ by using N-point FFT. Afterwards, the cross-correlation between the received preamble and the local known preamble in the frequency domain is calculated by

$$Q(m) = \frac{\sum_{k=0,\ \text{mod}\ (k,2)=0}^{2^{n+1}-2} \widetilde{q}_{m+k/2}^* \widetilde{u}_{k/2}}{2^n \alpha^2}, \quad \text{mod}\ (m,2) = 0, g_0 \leq m \leq g_0 + \frac{\Delta d}{2}, \quad (17)$$

where only the even subcarriers of the received frequency-domain preamble are used, and $\widetilde{\mathbf{u}} = \{\widetilde{u}_k\}_{k=0}^{2^n-1}$ denotes one possible Hadamard sequence candidate. Since there are two identical Hadamard sequences in the frequency-domain preamble, two correlation peaks are expected at the subcarrier locations k_1 and k_2 when the local Hadamard sequence matches the transmitted one, and the distance between the two correlation peaks should be $k_2 - k_1 = 2^{n+1} + \Delta d$. Finally, the system parameter signaling is detected by the sequence selection combined with the observed distance Δd, and the correct signaling can be used by the receiver for further processing.

B. Pilot-Based Residual CFO and Phase Noise Estimation

It is well known that the high-speed optical OFDM systems are sensitive to the phase noise caused by the unmatched transmit and receive lasers [26], [27]. Meanwhile, non-negligible residual CFO should be taken into account since the CFO during the preamble may not be the same as that during the following payload symbols. Considering the phase noise and the residual CFO, the nth received time-domain sample $\mathbf{r}_n^{(i)} = [r_{n,x}^{(i)}\ r_{n,y}^{(i)}]^T$ in the ith ZP-OFDM symbol should be [23]

$$\mathbf{r}_n^{(i)} = e^{j\theta_n^{(i)}} \sum_{l=0}^{L-1} \mathbf{H}_l^{(i)} \mathbf{s}_{n-l}^{(i)} + \mathbf{w}_n^{(i)}, \quad (18)$$

where $\theta_n^{(i)}$ denotes the composite time-varying effect of the phase rotation caused by the phase noise and the residual CFO, which is given by

$$\begin{cases} \theta_n^{(i)} = \phi_n^{(i)} + 2\pi n \omega T/N, \\ \phi_n^{(i)} = \phi_{n-1}^{(i)} + v_n^{(i)}, \end{cases} \quad (19)$$

where ω is the residual CFO normalized to the symbol rate $1/T$, $\phi_n^{(i)}$ denotes the time-varying phase noise subject to a Wiener model where v_n is a Gaussian variable with zero mean and variance dependent on the laser linewidth [28]. In high-speed optical OFDM systems, those time-varying impairments caused by the phase noise and the residual CFO, together with PMD,[5] would introduce ICI and consequently degrade the

[5]For high-speed optical OFDM systems, the ICI effect caused by PMD is usually negligible due to the slow time-varying nature of PMD, but the phase noise and the residual CFO may bring non-negligible ICI due to their relatively fast time-varying property [23].

system performance. The ICI effect on the frequency-domain received signal can be mathematically described by [23]

$$\widetilde{\mathbf{r}}_k^{(i)} = \Psi_0 \widetilde{\mathbf{H}}_k^{(i)} \widetilde{\mathbf{s}}_k^{(i)} + \underbrace{\sum_{l=0, l\neq k}^{L-1} \Psi_{k-l} \widetilde{\mathbf{H}}_l^{(i)} \widetilde{\mathbf{s}}_l^{(i)}}_{\text{ICI}} + \widetilde{\mathbf{w}}_k^{(i)}. \tag{20}$$

In the absence of phase noise, i.e., $\phi_n^{(i)}$ in (19) is constant so we have $\phi_n^{(i)} = \phi^{(i)}$, and the amplitude of the ICI coefficient caused by the residual CFO ω becomes

$$\begin{aligned} |\Psi_{k-l}| &= \left| \frac{1}{N} e^{j\phi^{(i)}} \sum_{n=0}^{N-1} e^{j\frac{2\pi}{N} n(\omega T - (k-l))} \right| \\ &= \frac{\sin\left(\pi\left(\omega T - (k-l)\right)\right)}{N \sin\left(\frac{\pi}{N}\left(\omega T - (k-l)\right)\right)}, \end{aligned} \tag{21}$$

which indicates that the major ICI is caused by the neighboring subcarriers when the residual CFO is present. For example, when the residual CFO equals 0.1 times of the subcarrier spacing $1/T$, i.e., $\omega T = 0.1$, we have $|\Psi_1| = 0.11$ and $|\Psi_2| = 0.05$. When $\omega T = 0.01$, the ICI effect becomes negligible since $|\Psi_k| < 0.01$ for all $|k| \geq 1$. As will be shown later in Section V, the CFO estimator (15) has excellent root mean squared error (RMSE) performance (e.g., the RMSE is as small as 0.0031 at the OSNR of 10 dB) due to the specially design preamble structure, so the residual CFO and the corresponding ICI should be very small. However, the obtained CFO estimate during the preamble may be outdated since the CFO may vary during the ZP-OFDM payload symbols. Thus residual CFO estimation is still required.

The ICI effect caused by the random time-varying phase noise is difficult to analyze in a closed-form as that for the residual CFO. However, the numerical results in [14] (and references therein) have demonstrated that even when the phase noise normalized to the symbol rate is as small as 2×10^{-4}, the resultant ICI is non-negligible. It is preferred in the proposed CO-ZP-OFDM scheme to estimate and then compensate for the phase noise before data detection in the frequency domain.

Similar to [6], [7], [12], [14], the pilots scattered in the ZP-OFDM symbols can also be used to estimate the residual CFO and the laser phase noise (the low-complexity linear interpolation can be used for the ZP-OFDM symbols without pilots). The only difference is that, in traditional CO-CP-OFDM systems [6], [7], [12], [14], the dedicated training symbols are used for channel estimation and some extra pilots are used for residual CFO and phase noise compensation, while our proposed method can simultaneously exploit the PTF-coded pilots for residual CFO estimation, phase noise compensation, and channel estimation as well. The channel estimation issue will be discussed in the following subsection.

C. Pilot-Based Polarization-Time-Frequency Channel Estimation

Based on the PTF-coded pilots, there are two ways to realize channel estimation for CO-ZP-OFDM systems.

1) *Polarization-Time Channel Estimation*

Based on the polarization-time orthogonal pilots (7) and the signal model (10), the received pilots $\left[\widetilde{d}_{k,x}^{(i)}\ \widetilde{d}_{k,y}^{(i)}\right]^T$ on the kth subcarrier in the ith ZP-OFDM symbol should be

$$\begin{bmatrix} \widetilde{d}_{k,x}^{(i)} \\ \widetilde{d}_{k,y}^{(i)} \end{bmatrix} = \begin{bmatrix} h_{k,xx}^{(i)} & h_{k,xy}^{(i)} \\ h_{k,yx}^{(i)} & h_{k,yy}^{(i)} \end{bmatrix} \begin{bmatrix} a \\ b \end{bmatrix} + \begin{bmatrix} \widetilde{w}_{k,x}^{(i)} \\ \widetilde{w}_{k,y}^{(i)} \end{bmatrix}, \tag{22}$$

and the received pilots $\left[\widetilde{d}_{k,x}^{(i+1)}\ \widetilde{d}_{k,y}^{(i+1)}\right]^T$ on the kth subcarrier in the $(i+1)$th ZP-OFDM symbol are

$$\begin{bmatrix} \widetilde{d}_{k,x}^{(i+1)} \\ \widetilde{d}_{k,y}^{(i+1)} \end{bmatrix} = \begin{bmatrix} h_{k,xx}^{(i+1)} & h_{k,xy}^{(i+1)} \\ h_{k,yx}^{(i+1)} & h_{k,yy}^{(i+1)} \end{bmatrix} \begin{bmatrix} c \\ d \end{bmatrix} + \begin{bmatrix} \widetilde{w}_{k,x}^{(i+1)} \\ \widetilde{w}_{k,y}^{(i+1)} \end{bmatrix}. \tag{23}$$

Since the optical fiber channel is slowly varying, i.e., $\widetilde{\mathbf{H}}_k^{(i)} = \widetilde{\mathbf{H}}_k^{(i+1)}$ could be assumed, the received pilots $\left[\widetilde{d}_{k,x}^{(i)}\ \widetilde{d}_{k,x}^{(i+1)}\right]^T$ in the x-polarization can be rewritten as

$$\begin{bmatrix} \widetilde{d}_{k,x}^{(i)} \\ \widetilde{d}_{k,x}^{(i+1)} \end{bmatrix} = \begin{bmatrix} a & b \\ c & d \end{bmatrix} \begin{bmatrix} h_{k,xx}^{(i)} \\ h_{k,xy}^{(i)} \end{bmatrix} + \begin{bmatrix} \widetilde{w}_{k,x}^{(i)} \\ \widetilde{w}_{k,x}^{(i+1)} \end{bmatrix}. \tag{24}$$

Therefore, $\left[h_{k,xx}^{(i)}\ h_{k,xy}^{(i)}\right]^T$ can be estimated by

$$\begin{aligned} \begin{bmatrix} \widehat{h}_{k,xx}^{(i)} \\ \widehat{h}_{k,xy}^{(i)} \end{bmatrix} &= \begin{bmatrix} a & b \\ c & d \end{bmatrix}^{-1} \begin{bmatrix} \widetilde{d}_{k,x}^{(i)} \\ \widetilde{d}_{k,x}^{(i+1)} \end{bmatrix} \\ &= \frac{1}{ad-bc} \begin{bmatrix} d & -b \\ -c & a \end{bmatrix} \begin{bmatrix} \widetilde{d}_{k,x}^{(i)} \\ \widetilde{d}_{k,x}^{(i+1)} \end{bmatrix}, \end{aligned} \tag{25}$$

which is simplified as

$$\begin{cases} \widehat{h}_{k,xx}^{(i)} = \frac{1}{2}\left(\widetilde{d}_{k,x}^{(i)} - \widetilde{d}_{k,x}^{(i+1)}\right) = h_{k,xx}^{(i)} + \frac{1}{2}\left(\widetilde{w}_{k,x}^{(i)} - \widetilde{w}_{k,x}^{(i+1)}\right), \\ \widehat{h}_{k,xy}^{(i)} = \frac{1}{2}\left(\widetilde{d}_{k,x}^{(i)} + \widetilde{d}_{k,x}^{(i+1)}\right) = h_{k,xy}^{(i)} + \frac{1}{2}\left(\widetilde{w}_{k,x}^{(i)} + \widetilde{w}_{k,x}^{(i+1)}\right), \end{cases} \tag{26}$$

when the simple pilot pattern $a = b = d = 1, c = -1$ is used.

Similarly, the channel estimates in the y-polarization take the form

$$\begin{cases} \widehat{h}_{k,yx}^{(i)} = \frac{1}{2}\left(\widetilde{d}_{k,y}^{(i)} - \widetilde{d}_{k,y}^{(i+1)}\right) = h_{k,yx}^{(i)} + \frac{1}{2}\left(\widetilde{w}_{k,y}^{(i)} - \widetilde{w}_{k,y}^{(i+1)}\right), \\ \widehat{h}_{k,yy}^{(i)} = \frac{1}{2}\left(\widetilde{d}_{k,y}^{(i)} + \widetilde{d}_{k,y}^{(i+1)}\right) = h_{k,yy}^{(i)} + \frac{1}{2}\left(\widetilde{w}_{k,y}^{(i)} + \widetilde{w}_{k,y}^{(i+1)}\right), \end{cases} \tag{27}$$

when the simple pilot pattern $a = b = d = 1, c = -1$ is used.

It is clear from (27) that the noise has been averaged, i.e., the noise variance is halved and the equivalent OSNR for channel estimation is increased by 3 dB, so diversity gain can be achieved by the polarization-time channel estimation.

2) *Polarization-Frequency Channel Estimation*

Starting from the polarization-frequency orthogonal pilot model (8), and considering the kth and the $(k+1)$th subcarriers in the ith ZP-OFDM symbol, one can easily obtain the following channel estimates

$$\begin{cases} \widehat{h}_{k,xx}^{(i)} = \frac{1}{2}\left(\widetilde{d}_{k,x}^{(i)} - \widetilde{d}_{k+1,x}^{(i)}\right) = h_{k,xx}^{(i)} + \frac{1}{2}\left(\widetilde{w}_{k,x}^{(i)} - \widetilde{w}_{k+1,x}^{(i)}\right), \\ \widehat{h}_{k,xy}^{(i)} = \frac{1}{2}\left(\widetilde{d}_{k,x}^{(i)} + \widetilde{d}_{k+1,x}^{(i)}\right) = h_{k,xy}^{(i)} + \frac{1}{2}\left(\widetilde{w}_{k,x}^{(i)} + \widetilde{w}_{k+1,x}^{(i)}\right), \end{cases} \tag{28}$$

$$\begin{cases} \widehat{h}_{k,yx}^{(i)} = \frac{1}{2}\left(\widetilde{d}_{k,y}^{(i)} - \widetilde{d}_{k+1,y}^{(i)}\right) = h_{k,yx}^{(i)} + \frac{1}{2}\left(\widetilde{w}_{k,y}^{(i)} - \widetilde{w}_{k+1,y}^{(i)}\right), \\ \widehat{h}_{k,yy}^{(i)} = \frac{1}{2}\left(\widetilde{d}_{k,y}^{(i)} + \widetilde{d}_{k+1,y}^{(i)}\right) = h_{k,yy}^{(i)} + \frac{1}{2}\left(\widetilde{w}_{k,y}^{(i)} + \widetilde{w}_{k+1,y}^{(i)}\right), \end{cases} \tag{29}$$

TABLE I
COMPARISON OF PILOT OCCUPATION RATIO.

Transmission Scheme	Pilot Occupation Ratio
Conventional CO-CP-OFDM [16]	9.16%
Proposed CO-ZP-OFDM	2.48%

under the assumption of $\widetilde{\mathbf{H}}_k^{(i)} = \widetilde{\mathbf{H}}_{k+1}^{(i)}$ and when the simple pilot pattern $a = b = d = 1, c = -1$ is used. It is observed that 3 dB gain is also achieved with this scheme.

Based on the fact that the optical channel has flat CFR and slow time-varying properties, both the polarization-time and polarization-frequency channel estimation methods can be used to acquire the CFR over the PTF-coded pilots. Then, the CFR over the data subcarriers can be obtained by the low-complexity linear interpolation. In addition, the pilot power boosting method can further improve the channel estimation performance.

D. Channel Equalization and LDPC Decoding

After timing/frequency synchronization and phase noise compensation, the OLA method [25] is used to reconstruct the cyclicity of the received IFFT data block in each ZP-OFDM symbol, so that the obtained channel information above can be used to compensate for the optical impairments via channel equalization. Then, the estimated constellation symbols are fed into *a posterior* probability demapper, wherein the bit log likelihood ratio (LLR) for each constellation symbol can be calculated in both x- and y-polarizations according to [29]. Then, the initial LLR is computed by [29]

$$\mathrm{LLR}(\widetilde{s}_{k,x,j}^{(i)}) = \log \frac{p(\widetilde{s}_{k,x,j}^{(i)} = 0 | \widetilde{v}_{k,x,j}^{(i)})}{p(\widetilde{s}_{k,x,j}^{(i)} = 1 | \widetilde{v}_{k,x,j}^{(i)})},$$

where $\widetilde{v}_{k,x,j}^{(i)}$ denotes jth bit of the estimated symbol $\widetilde{v}_{k,x}^{(i)}$ corresponding to the jth bit $\widetilde{s}_{k,x,j}^{(i)}$ of the transmitted symbol $\widetilde{s}_{k,x}^{(i)}$, and the LLR will be used for the sum-product algorithm (SPA) [30], [31] for LDPC decoding to output the final decoded information bits.

IV. PERFORMANCE ANALYSIS

This section analyzes the performance of the proposed CO-ZP-OFDM transmission scheme in terms of spectral efficiency, equivalent OSNR variation caused by ZP insertion/pilot power boosting, and the computational complexity. Extension of the proposed scheme to other high-speed optical transport systems is also presented.

A. Spectral Efficiency

Insertion of training symbols and frequency-domain pilots in a CO-CP-OFDM system would reduce the spectral efficiency. For the proposed CO-ZP-OFDM scheme, as illustrated by Fig. 4, the pilot occupation ratio η is

$$\eta = \frac{4 \times 3}{(2 \times 3 + \Delta i \times 2) \times (2 \times 3 + \Delta k \times 2)} \times 100\%. \quad (30)$$

Table I compares the pilot occupation ratio between a typical CO-CP-OFDM system and the proposed CO-ZP-OFDM scheme. The typical values $N = 2048, M = 256$ are used for both schemes. In CO-CP-OFDM, a pair of training symbols are inserted after every 20 CP-OFDM payload symbols [16] for channel tracking, and usually 16 extra frequency-domain pilots in each symbol are used for residual CFO and phase noise estimation [13]. So the pilot occupation ratio is 9.16%. For the proposed CO-ZP-OFDM scheme, the PTF-coded pilots with the frequency-domain distance $\Delta k = 8$ and time-domain distance $\Delta i = 8$ are sufficient to track the channel variation, and those pilots are simultaneously used for residual CFO and phase noise compensation. So the pilot occupation ratio is only 2.48%. Therefore, CO-ZP-OFDM has higher spectral efficiency than CO-CP-OFDM.

Note that more PTF coded pilots should be used by the proposed CO-ZP-OFDM scheme when the optical channel has more ripples in the frequency domain. However, even in this case, CO-ZP-OFDM still has higher spectral efficiency than the conventional CO-CP-OFDM scheme using one or several complete OFDM training symbols for channel tracking.

TABLE II
COMPARISON OF OSNR PENALTY DUE TO PILOT POWER BOOSTING.

β	$\Delta\mathrm{OSNR}_2$ for CO-CP-OFDM	$\Delta\mathrm{OSNR}_2$ for CO-ZP-OFDM
$\sqrt{2}$	0.38 dB	0.11 dB
2	1.05 dB	0.31 dB
$2\sqrt{2}$	2.15 dB	0.70 dB

B. Equivalent OSNR Variation

Compared with CO-CP-OFDM, the OSNR at the CO-ZP-OFDM optical receiver would vary due to ZP insertion and pilot power boosting.

Another difference between CO-CP-OFDM and CO-ZP-OFDM is that, CP has the similar average power as the IFFT data block, while ZP has zero power. Consequently, the power originally allocated to CP in CO-CP-OFDM can now be added to the useful IFFT data block in CO-ZP-OFDM without changing the total transmission power. Therefore, transmission power can be used more efficiently by CO-ZP-OFDM. Accordingly, it would increase the equivalent OSNR at the optical CO-ZP-OFDM receiver by

$$\Delta\mathrm{OSNR}_1 = 10\log_{10}\left(\frac{M+N}{N}\right). \quad (31)$$

For example, an equivalent OSNR gain of 0.51 dB can be achieved by using ZP as the guard interval when $M = N/8$.

On the other hand, the pilot power boosting would reduce the equivalent OSNR at the optical receiver by

$$\Delta\mathrm{OSNR}_2 = 10\log_{10}\left(\eta\beta^2 + (1-\eta)\right), \quad (32)$$

where η is the pilot occupation ratio defined in (30), β denotes the amplitude scaling factor used to boost the pilot power (for most OFDM systems, the useful data power is usually normalized to 1 at the transmitter).

Table II lists the OSNR loss when different pilot power levels are used. For CO-ZP-OFDM, it is clear that when the pilot power is 6 dB ($\beta = 2$) higher than the normal data, the OSNR loss is only 0.31 dB at the receiver. Note that

pilot power boosting could also be used by the periodically inserted training symbols in common CO-CP-OFDM systems to improve the receiver performance, but high pilot occupation ratio would result in obvious OSNR loss, e.g., the OSNR loss is 1.05 dB when $\beta = 2$. Instead, pilot power boosting in the proposed CO-ZP-OFDM scheme helps to improve channel estimation and residual CFO/phase noise compensation performance without obvious decrease of the equivalent OSNR.

C. Computational Complexity

The CO-CP-OFDM and CO-ZP-OFDM schemes also differ in receiver signal processing aspects: the joint timing/frequency synchronization and signaling detection using the preamble, the PTF channel estimation exploiting the PTF-coded pilots, and the OLA algorithm used to reconstruct the cyclicity of the received IFFT data block in CO-ZP-OFDM.

For correlation-based timing synchronization (12) and CFO estimation (15), computation of the correlation function is similar to that used in a CO-CP-OFDM system even though the proposed preamble can improve the synchronization performance [14], [17]. Thus, two schemes share the same complexity for timing/frequency synchronization. But the proposed preamble can also be used for signaling detection at very low complexity, because the multiplication required to calculate the cross-correlation function (16) in the frequency domain is simplified to direct addition/subtraction by the real-valued Hadamard sequence.

When the PTF-coded pilots are simply selected from the BPSK constellation, both the polarization-time channel estimation (27) and the polarization-frequency channel estimation (29) can be realized by simple addition/subtraction. Therefore, PTF channel estimation has very low complexity, similar to that in a CO-CP-OFDM system [12], [15], [17].

The OLA algorithm [25] also has low complexity, since Fig. 7 indicates that it only requires to add the "tail" caused by the multipath effect to the front part of the received IFFT data block.

In summary, CO-ZP-OFDM and CO-CP-OFDM have similar yet low computational complexity.

D. Extension to Other Optical Communication Systems

The proposed CO-ZP-OFDM scheme, or some key components of this scheme, can be directly used or easily extended to other optical communication systems.

First, the flexible transmission frame structure is applicable to CO-CP-OFDM systems after a simple modification: replacing ZP with CP. As a result, the OLA method is not necessary any more. However, most of other key components of the proposed CO-ZP-OFDM scheme, including the signaling-embedded preamble design and the corresponding joint timing/frequency synchronization and signaling detection method, the PTF-coded pilots design and the corresponding reliable PTF channel estimation, can be directly used by CO-CP-OFDM to achieve higher spectral efficiency and more accurate synchronization/channel estimation.

Second, the proposed signaling-embedded preamble with Delta-like timing metric can be directly used by coherent optical single-carrier frequency domain equalization (CO-SC-FDE) systems to improve the timing synchronization performance. In addition, its capability of conveying the system parameters can be exploited to reliably deliver physical layer signaling without any extra overhead.

Third, when the proposed scheme is simplified to a multiple-input single-output (MISO) case, the PTF coded pilots can be directly used to separate the polarization specific channel, while in a single-input multiple-output (SIMO) system, e.g. the PDM at the transmitter is not considered, the PTF coded pilots will be reduced to the single pilot tone commonly used in an OFDM system [4], [13].

In addition, it is well-known that the MIMO technique could be used in two different ways [32]–[34]: increasing the system transmission capacity by means of multiplexing, e.g., the PDM discussed in this paper, or improving the transmission reliability via diversity, e.g., the Alamouti-type polarization-time coding schemes [28], [35]. Strictly speaking, the design of the PTF-coded pilots in Fig. 4 is based on the Alamouti-type diversity principle, while PDM is achieved by the multiplexing principle. Therefore, two different merits of the MIMO technique have been concurrently exploited in the proposed scheme. Note that the PTF-coded pilots in this paper are also applicable to other MIMO systems where diversity instead of multiplexing is used to transmit the useful data.

V. Numerical Results and Discussions

In this section, the performance of the proposed flexible CO-ZP-OFDM transmission based on signaling-embedded preamble and PTF-coded pilots is numerically evaluated using Matlab. The simulation setup is similar to the PDM OFDM system in [16]: The IFFT length is 2048, the ZP length is 512; The transmission link is composed of 16 optically amplified 80-km fiber spans, and the electronic dispersion compensation (EDC) via one-tap filter is performed prior to channel estimation at the receiver; The channel impairments like CD, PMD, PDL, and fiber nonlinearity are all taken into account; The optical CD of 2,000 ps/nm or 8,000 ps/nm is considered. The PMD with the mean differential group delay (denoted by $\langle \mathrm{DGD} \rangle$) of 100 ps or 400 ps is incorporated;[6] The fiber nonlinear coefficient of 1.22/W/km is considered; The noise figure of the EDFA is 4.5 dB. Refer to [16] for more details of the simulation setup. The amplitude factor used to boost the pilot power is set as $\beta = 2$. The constellation scheme 16QAM is adopted. We choose the LDPC code in [28] due to its low complexity and very low error floor resulted from the absence of 4-cycles in its graph [36]. The SPA decoding scheme is adopted for iterative soft-decision decoding with the iteration number of 50 [31]. The polarization-diversity optical hybrid detector has the optical local oscillator with the line bandwidth of 100 kHz. The OSNR at the receiver is defined with the 0.1 nm noise bandwidth.

Figure 8 compares the timing metric behavior of the proposed preamble with those of the classical Schmidl's and Minn's preambles in the absence of noise and channel

[6]Strictly speaking, DGD is subject to a Maxellian distribution since PMD is a stochastic process. So the instantaneous DGD maybe much larger than $\langle \mathrm{DGD} \rangle$ but with very low probability [16].

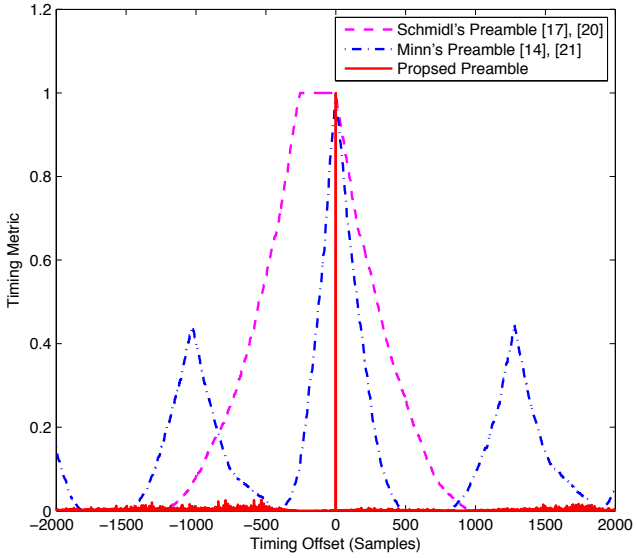

Fig. 8. Comparison of the timing metric behaviors in the absence of noise and channel distortion. The timing offset 0 indicates the exact timing point.

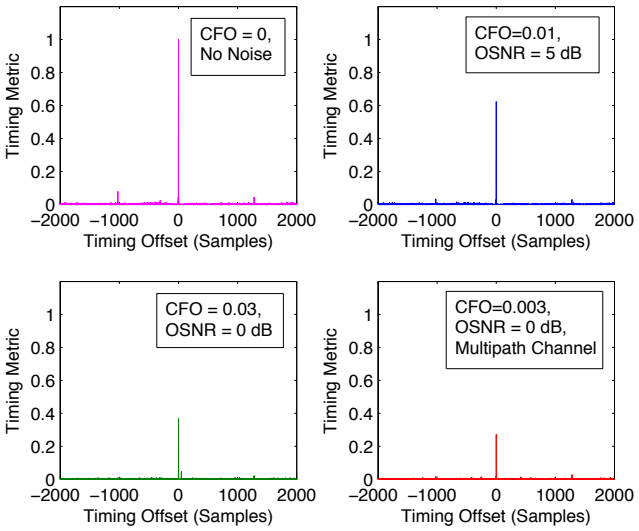

Fig. 9. Timing metric of the proposed preamble under different CFOs and OSNRs. The first three subplots are obtained over an AWGN channel, while the last subplot over a multipath channel.

distortion. A plateau for Schmidl's preamble [17], [20] is observed, and much sharper timing metric is achieved by Minn's preamble [14], [21]. However, neither of them is as sharp as the proposed preamble that enjoys the ideal Delta-like timing metric, indicating that very precise timing synchronization can be achieved by the proposed preamble both in the singlepath and multipath channels.

The robustness of the timing metric to CFO is usually desirable. It is examined by Figure 9 that shows the impact of the normalized CFOs on the timing metric under different conditions. The timing metric is still a Delta-like function which indicates that successful timing synchronization can be achieved even with CFO distortion.

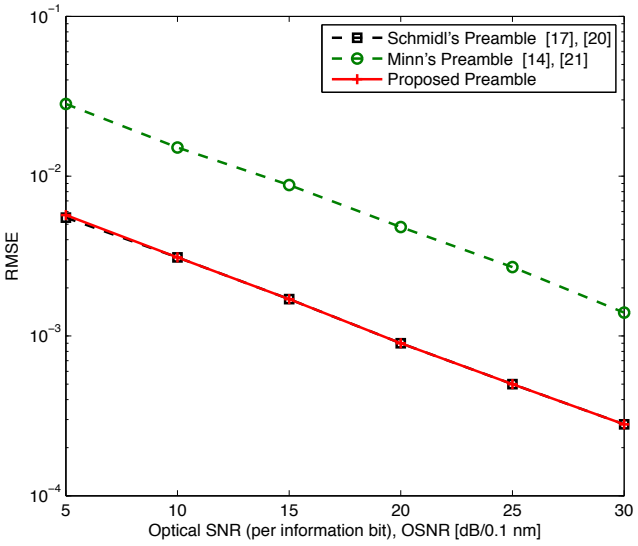

Fig. 10. Comparison of the RMSE performance of the normalized CFO estimation.

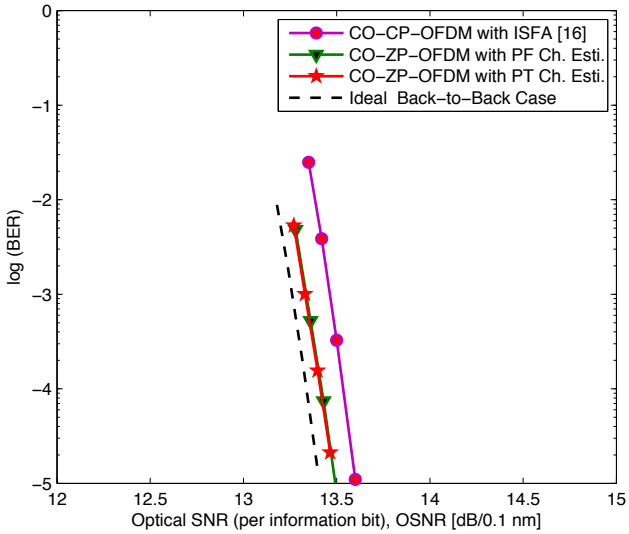

Fig. 11. Coded BER performance comparison with the CD of 2,000 ps/nm and $\langle \mathrm{DGD} \rangle$ of 100 ps.

Figure 10 compares the RMSE performance of the normalized CFO estimator (15) with those of the conventional schemes. We can observe that the proposed CFO estimator performs similarly as Schmidl's method [20] but much better than Minn's solution [21]. The CFO can be estimated at a very small error, for example, the RMSE is 0.0031 when OSNR is 10 dB.

Figure 11 shows the coded bit error rate (BER) performance of the proposed CO-ZP-OFDM scheme with the CD of 2,000 ps/nm and $\langle \mathrm{DGD} \rangle$ of 100 ps. For comparison, we also present the BER performance of the conventional CO-CP-OFDM system with reliable performance [16], where the ISFA method implements the frequency-domain averaging among several neighboring subcarriers in the same training symbol to improve the performance. We select this method

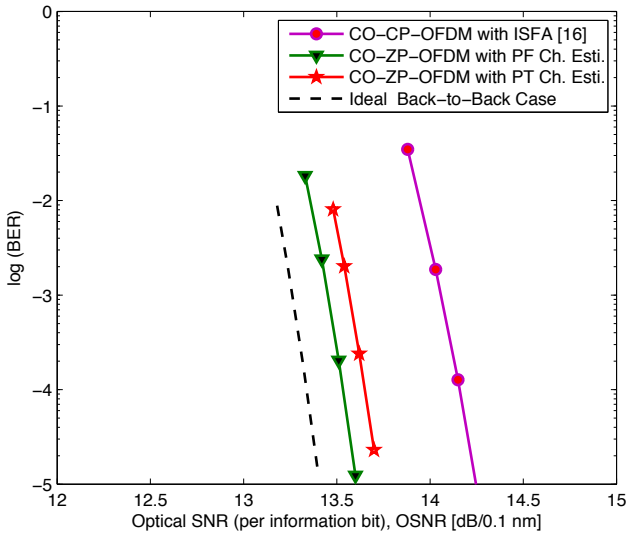

Fig. 12. Coded BER performance comparison with the CD of 8,000 ps/nm and $\langle \mathrm{DGD} \rangle$ of 400 ps.

to compare because it achieves similar reliable performance by time-domain averaging as its peers, but requires much fewer training symbols [37]. The BER in the ideal back-to-back (B2B) case where the channel has no distortion but with optical noise, is used as the comparison benchmark. The small CD indicates that the optical channel in each ZP-OFDM symbol does not fluctuate much in the frequency domain, and the relatively small $\langle \mathrm{DGD} \rangle$ means that the channel is varying slowly in the time domain. We can observe from Fig. 11 that the conventional CO-CP-OFDM system and the proposed CO-ZP-OFDM scheme have similar BER performance in this case. For CO-ZP-OFDM, the polarization-time channel estimation (denoted by "PT Ch. Esti.") has very close performance to that of the polarization-frequency channel estimation (denoted by "PF Ch. Esti."). They both perform slightly better than CO-CP-OFDM with the OSNR gain of 0.1 dB, and enjoy less than 0.1 dB OSNR penalty with respect to the B2B case. As CD increases to 8,000 ps/nm and big $\langle \mathrm{DGD} \rangle$ to 400 ps, both of the polarization-frequency channel estimation and the polarization-time channel estimation perform much better than CO-CP-OFDM, and only suffer from no more than 0.3 dB compared with the ideal B2B case. These are demonstrated by Figure 12.

VI. Conclusions

In this paper, the CO-ZP-OFDM transmission scheme with signaling-embedded preamble and PTF-coded pilots was proposed for future spectrum-efficient and elastic optical transport networks. The signaling-embedded preamble helps to simultaneously achieve accurate timing/frequency synchronization as well as system parameter signaling detection. The reliable PTF channel estimation was realized by the PTF-coded pilots, which could also be used for residual CFO and phase noise compensation. The proposed CO-ZP-OFDM scheme has higher spectral efficiency than CO-CP-OFDM, and demonstrates reliable performance even under severe CD and PMD conditions. It can be easily extended to other CO-OFDM and CO-SC-FDE systems to improve the spectral efficiency and enhance the performance. Moreover, the proposed CO-ZP- OFDM scheme can be combined with OBM technique to provide the data rate up to Tb/s for future optical transport networks.

Acknowledgement

The authors would like than thank Dr. He Wen and Dr. Ying Zhao for their valuable discussions and helpful suggestions.

References

[1] G. Shen and Q. Yang, "From coarse grid to mini-grid to gridless: How much can gridless help contentionless?" in *Optical Fiber Communinications Conference (OFC)*, Mar. 2011.
[2] A. R. Dhaini, P.-H. Ho, and G. Shen, "Toward green next-generation passive optical networks (NG-PONs)," *IEEE Commun. Mag.*, vol. 49, no. 11, pp. 94–101, Nov. 2011.
[3] W. Shieh, H. Bao, and Y. Tang, "Coherent optical OFDM: Theory and design," *Opt. Express*, vol. 16, no. 2, pp. 841–859, Jan. 2008.
[4] W. Shieh and C. Athaudage, "Coherent optical orthogonal frequency division multiplexing," *Electron. Lett.*, vol. 42, no. 10, pp. 587–589, May 2006.
[5] G. Shen, S. You, Q. Yang, Z. He, N. Yang, Z. Yang, S. Yu, and W. Shieh, "Experimental demonstration of CO-OFDM optical network with heterogeneous ROADM nodes and variable channel bit-rates," *IEEE Commun. Lett.*, vol. 15, no. 8, pp. 890–892, Aug. 2011.
[6] W. Shieh, X. Yi, Y. Ma, and Y. Tang, "Theoretical and experimental study on PMD-supported transmission using polarization diversity in coherent optical OFDM systems," *Opt. Express*, vol. 15, no. 16, pp. 9936–9947, July 2007.
[7] S. Jansen, I. Morita, T. Schenk, N. Takeda, and H. Tanaka, "Coherent optical 25.8-Gb/s OFDM transmission over 4160-km SSMF," *J. Lightwave Technol.*, vol. 26, no. 1, pp. 6–15, Feb. 2008.
[8] W. Shieh, Q. Yang, and Y. Ma, "107 Gb/s coherent optical OFDM transmission over 1000-km SSMF fiber using orthogonal band multiplexing," *Opt. Express*, vol. 16, no. 9, pp. 6378–6386, Apr. 2008.
[9] W. Shieh, "High spectral efficiency coherent optical OFDM for 1 Tb/s Ethernet transport," in *Optical Fiber Communinications Conference (OFC)*, Mar. 2009.
[10] S. Jansen, I. Morita, and H. Tanaka, "10x121.9-Gb/s PDM-OFDM transmission with 2-b/s/Hz spectral efficiency over 1,000 km of SSMF," in *Optical Fiber Communinications Conference (OFC)*, Mar. 2008.
[11] S. Jansen, I. Morita, T. Schenk, and H. Tanaka, "121.9-Gb/s PDM-OFDM transmission with 2-b/s/Hz spectral efficiency over 1000 km of SSMF," *J. Lightwave Technol.*, vol. 27, no. 3, pp. 177–188, Jan. 2009.
[12] ——, "Long-haul transmission of 16×52.5 Gbits/s polarization-division-multiplexed OFDM enabled by MIMO processing," *J. Opt. Netw.*, vol. 7, no. 2, pp. 173–182, Feb. 2008.
[13] F. Buchali, R. Dischler, and X. Liu, "Optical OFDM: A promising high-speed optical transport technology," *Bell Labs Tech. J.*, vol. 14, no. 1, pp. 125–146, Jan. 2009.
[14] S. Chen, Q. Yang, Y. Ma, and W. Shieh, "Real-time multi-Gigabit receiver for coherent optical MIMO-OFDM signals," *J. Lightwave Technol.*, vol. 27, no. 16, pp. 3699–3704, Aug. 2009.
[15] X. Liu and F. Buchali, "A novel channel estimation method for PDM-OFDM enabling improved tolerance to WDM nonlinearity," in *Optical Fiber Communinications Conference (OFC)*, Mar. 2009.
[16] ——, "Intra-symbol frequency-domain averaging based channel estimation for coherent optical OFDM," *Opt. Express*, vol. 16, no. 26, pp. 21 944–21 957, Dec. 2008.
[17] C. Youn, X. Liu, S. Chandrasekhar, Y. Kwon, J. Kim, J. Choe, D. Kim, K. Choi, and E. Nam, "Channel estimation and synchronization for polarization-division multiplexed CO-OFDM using subcarrier/polarization interleaved training symbols," *Opt. Express*, vol. 19, no. 17, pp. 16 174–16 181, Aug. 2011.
[18] H. Sun, K. Wu, and K. Roberts, "Real-time measurements of a 40 Gb/s coherent system," *Opt. Express*, vol. 16, no. 2, pp. 873–879, Jan. 2008.
[19] C. yen Ong, J. Song, C. Pan, and Y. Li, "Technology and standards of digital television terrestrial multimedia broadcasting," *IEEE Commun. Mag.*, vol. 48, no. 5, pp. 119–127, May 2010.
[20] T. Schmidl and D. Cox, "Robust frequency and timing synchronization for OFDM," *IEEE Trans. Commun.*, vol. 45, no. 12, pp. 1613–1621, Dec. 1997.

[21] H. Minn, V. K. Bhargava, and K. B. Letaief, "A robust timing and frequency synchronization for OFDM systems," *IEEE Trans. Wireless Commun.*, vol. 2, no. 4, pp. 822–839, July 2003.
[22] K. Kwak, S. Lee, D. Hong, and J. Kim, "A new DFT-based channel estimation approach for OFDM with virtual subcarriers by leakage estimation," *IEEE Trans. Wireless Commun.*, vol. 7, no. 6, pp. 2004–2008, June 2008.
[23] A. Barbieri, G. Colavolpe, T. Foggi, E. Forestieri, and G. Prati, "OFDM versus single-carrier transmission for 100 Gbps optical communication," *J. Lightwave Technol.*, vol. 28, no. 17, pp. 2537–2551, Sept. 2010.
[24] G. Colavolpe, T. Foggi, E. Forestieri, and G. Prati, "Robust multilevel coherent optical systems with linear processing at the receiver," *J. Lightwave Technol.*, vol. 27, no. 13, pp. 2357–2369, July 2009.
[25] B. Muquet, Z. Wang, G. Giannakis, M. De Courville, and P. Duhamel, "Cyclic prefixing or zero padding for wireless multicarrier transmissions?" *IEEE Trans. Commun.*, vol. 50, no. 12, pp. 2136–2148, Dec. 2002.
[26] C. Yang, F. Yang, and Z. Wang, "Orthogonal basis expansion-based phase noise estimation and suppression for CO-OFDM systems," *IEEE Photon. Technol. Lett.*, vol. 22, no. 1, pp. 51–53, Jan. 2010.
[27] ——, "Phase noise suppression for coherent optical block transmission systems: A unified framework," *Opt. Express*, vol. 19, no. 18, pp. 17 013–17 020, Aug. 2011.
[28] I. Djordjevic, L. Xu, and T. Wang, "Alamouti-type polarization-time coding in coded-modulation schemes with coherent detection," *Opt. Express*, vol. 16, no. 18, pp. 14 163–14 172, Aug. 2008.
[29] I. Djordjevic, S. Sankaranarayanan, S. Chilappagari, and B. Vasic, "Low-density parity-check codes for 40-Gb/s optical transmission systems," *IEEE J. Sel. Topics Quantum Electron.*, vol. 12, no. 4, pp. 555–562, Aug. 2006.
[30] D. MacKay, "Encyclopedia of sparse graph codes," *[Online] http://wol.ra.phy.cam.ac.uk/mackay/codes*, 2005.
[31] R. Neal, "Software for low density parity check codes," *Freeware on the Internet, web address http://www.cs.toronto.edu/pub/radford/LDPC-2001-11-18/index.html*, 2006.
[32] L. Zheng and D. Tse, "Diversity and multiplexing: A fundamental tradeoff in multiple-antenna channels," *IEEE Trans. Inf. Theory*, vol. 49, no. 5, pp. 1073–1096, May 2003.
[33] D. Tse, P. Viswanath, and L. Zheng, "Diversity-multiplexing tradeoff in multiple-access channels," *IEEE Trans. Inf. Theory*, vol. 50, no. 9, pp. 1859–1874, Sept. 2004.
[34] M. Yuksel and E. Erkip, "Multiple-antenna cooperative wireless systems: A diversity–multiplexing tradeoff perspective," *IEEE Trans. Inf. Theory*, vol. 53, no. 10, pp. 3371–3393, Oct. 2007.
[35] W. Peng, K. Feng, and S. Chi, "Joint compensation of CD and PMD in direct-detected OFDM transmission using polarization-time coding," *Opt. Express*, vol. 18, no. 3, pp. 1916–1926, Jan. 2010.
[36] M. Sakib, V. Mahalingam, W. Gross, and O. Liboiron-Ladouceur, "Optical front-end for soft-decision LDPC codes in optical communication systems," *IEEE/OSA J. Opt. Commun. Netw.*, vol. 3, no. 6, pp. 533–541, 2011.
[37] Q. Yang, N. Kaneda, X. Liu, and W. Shieh, "Demonstration of frequency-domain averaging based channel estimation for 40-Gb/s CO-OFDM with high PMD," *IEEE Photon. Technol. Lett.*, vol. 21, no. 20, pp. 1544–1546, Oct. 2009.

Linglong Dai (M'11) received his B.S. degree from Zhejiang University in 2003, M.S. degree (with the highest honor) from China Academy of Telecommunications Technology (CATT) in 2006, and Ph.D. degree (with the highest honor) from Tsinghua University in 2011, respectively. He is now a Post Doctoral Fellow with the Department of Electronic Engineering, Tsinghua University, Beijing, China. His research focuses on wireless and optical communications. He has published over 20 journal and conference papers. He was awarded the 2011 Tsinghua Excellent Doctor of Electronic Engineering, the 2011 Tsinghua Academic Star, and the 2012 Beijing Excellent Doctoral Dissertations.

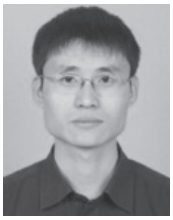

Chao Zhang (M'09) received his B. Eng and Ph.D degrees in 2001 and 2008 respectively, from School of Electronic and Information Engineering, Beijing University of Aeronautics and Astronautics. He is now the research assistant in Department of Electronic Engineering of Tsinghua University. His primary research interests focus on broadband wireless communication and digital television broadcasting, especially synchronization, channel estimation and single carrier frequency domain equalization.

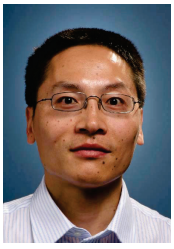

Zhengyuan Xu (S'97-M'99-SM'02) received his B.S. and M.S. degrees in electronic engineering from Tsinghua University, Beijing, China, in 1989 and 1991, respectively, and Ph.D. degree in electrical engineering from Stevens Institute of Technology, Hoboken, NJ, in 1999. From 1991 to 1996, he was with Tsinghua Unisplendour Group Corporation, Tsinghua University, as system engineer and department manager. In 1999, he joined University of California, Riverside, first as Assistant Professor and then tenured Associate Professor and Professor. He was Founding Director of the multi-campus Center for Ubiquitous Communication by Light (UC-Light), University of California. In 2010, he was selected by the "Thousand Talents Program" of China, and appointed as Professor in Department of Electronic Engineering and Tsinghua National Laboratory for Information Science and Technology, Tsinghua University, where he has established Optical Wireless Information Systems (OWisys) Laboratory. His research focuses on wireless communications, networking, optical wireless communications, geolocation, and intelligent transportation systems. He has published over 160 journal and conference papers.

He has served as an associate editor and guest editor for different IEEE journals in communications, vehicular technology, or signal processing. He also served as a chair, session chair, technical program committee chair and member for numerous international conferences and workshops. He was Founding Chair of IEEE Workshop on Optical Wireless Communications and IEEE International Workshop on Optical Wireless Communications in China. He was an elected member of IEEE Signal Processing Society's Technical Committee on Signal Processing for Communications for several years.

Zhaocheng Wang (M'06-SM'11) received his B.S., M.S. and Ph.D. degrees from Tsinghua University in 1991, 1993 and 1996, respectively. From 1996 to 1997, he was with Nanyang Technological University (NTU) in Singapore as a Post Doctoral Fellow. From 1997 to 1999, he was with OKI Techno Centre (Singapore) Pte. Ltd., firstly as a research engineer and then as a senior engineer. From 1999 to 2009, he worked at SONY Deutschland GmbH, firstly as a senior engineer and then as a principal engineer. He is currently a Professor at the Department of Electronic Engineering, Tsinghua University. His research areas include wireless communications, digital broadcasting and millimeter wave communications. He holds 25 granted US/EU patents and has published over 70 technical papers. He has served as technical program committee co-chair/member of many international conferences. He is a Senior Member of IEEE and a Fellow of IET.